Disruption of conserved polar interactions causes a sequential release of Bim mutants from the canonical binding groove of Mcl1

Parthiban Marimuthu[1†], Jamoliddin Razzokov[2], Gofur Eshonqulov[3]

[1]Structural Bioinformatics Laboratory (SBL), Biochemistry and Pharmacy, Faculty of Science and Engineering, Åbo Akademi University, FI-20520 Turku, Finland.

[2]Research Group PLASMANT, Department of Chemistry, University of Antwerp, Universiteitsplein 1, B-2610, Antwerp, Belgium.

[3]Department of Physics, National University of Uzbekistan, 100174, Tashkent, Uzbekistan.

[†]Address correspondence to:

Dr. Parthiban Marimuthu (Ph.D.), Structural Bioinformatics Laboratory (SBL), Biochemistry, Faculty of Science and Engineering, Åbo Akademi University, Tykistökatu 6A, FI-20520 Turku, Finland. Phone: +358 2 215 4600, E-mail address:

parthiban.marimuthu@abo.fi

Abstract

Mcl1 is an important anti-apoptotic member of the Bcl2 family proteins that are upregulated in several cancer malignancies. The canonical binding groove (CBG) located at the surface of Mcl1 exhibits a critical role in binding partners selectively via the BH3-domain of pro-apoptotic Bcl2 family members that trigger the downregulation of Mcl1 function. There are several crystal structures of point-mutated pro-apoptotic Bim peptides in complex with Mcl1. However, the mechanistic effects of such point-mutations towards peptide binding and complex stability still remain unexplored. Here, the effects of the reported point mutations in Bim peptides and their binding mechanisms to Mcl1 were computationally evaluated using atomistic-level steered molecular dynamics (SMD) simulations. A range of external-forces and constant-velocities were applied to the Bim peptides to uncover the mechanistic basis of peptide dissociation from the CBG of Mcl1. Although the peptides showed similarities in their dissociation pathways, the peak rupture forces varied significantly. According to simulations results, the disruption of the conserved polar contacts at the complex interface causes a sequential release of the peptides from the CBG of Mcl1. Overall, the results obtained from the current study may provide valuable insights for the development of novel anti-cancer peptide-inhibitors that can downregulate Mcl1's function.

Introduction

Apoptosis is a programmed cell death, which is one of the crucial regulatory process essential for immunity, tissue development and homeostasis [1]. The members of B-cell lymphoma 2 (Bcl-2) protein family play a central role in closely monitoring the apoptotic process *via* the intrinsic pathway in the outer membrane of mitochondria [2]. The Bcl-2 family members share up to four structurally similar domain regions (BH1 to BH4) known as Bcl-2 homology (BH) domains [3]. These domain regions determine the function of the protein family members to exhibit: (i) anti-apoptotic (AA) activity — promote cell survival (Bcl-2, Bcl-xL, Bcl-W, Bcl-B, Mcl1 and Bfl-1/A1 proteins); (ii) pro-apoptotic (PA) activity which leads to induction of pore formation at the outer membrane of mitochondria (Bax, Bak and Bok proteins); and (iii) direct activation of oligomerization (also PA activity) (BH3-only proteins: Bim, Bid, Bik, Bad, Bmf, Hrk, Noxa and Puma) [4].

Several studies have revealed that the Bcl-2 family proteins are comprised of multiple α-helices (α_1 to α_9) and can contain multiple BH domains [5-7]. These α-helices are tightly assembled to form a unique "canonical binding groove" (CBG) juxtaposed to the BH1–3 domains located at the surface of the Bcl-2 proteins [8]. To regulate apoptosis, the CBG of one family type (e.g. AA) proteins can attract the α-helical BH3 domain of the other types of proteins (e.g. PA and BH3-only) [9]. Thus, the BH3 domains of the Bcl-2 family members play an important role in apoptosis *via* protein-protein interactions to govern the cell's fate [9]. The binding properties of BH3 domains are utilized to develop novel/modified amphipathic α-helical peptides [10] as chemical inhibitors [11].

The CBG exhibits remarkable selectivity, i.e., the binding partners' (the α-helical

3

BH3 domains) binding is highly specific among the family proteins (though with a wide range of binding affinities) [12, 13]. Certain PA members of the protein family, e.g., BH3 domains of Bim and Puma exhibit promiscuity towards AA members of the family with low binding affinity values [14] while other PA members, e.g., Bad and Noxa show high specificity in binding to AA proteins (low nM) [15, 16]. These differences in selectivity explain why only certain combinations of α-helical peptide regions have the ability to kill cells. A strong apoptotic interaction between AA and PA proteins takes place when a combination of hydrophobic side chains at 2a, 3a, 3d, 4a and 4e positions (Figure 1a) of PA peptides inserts into the small sub-pockets located inside the CBG of AA proteins.

There is an extreme demand for novel high-affinity peptides that specific to individual family members. Among the AA proteins, Mcl1 is intensively studied as an attractive target for anticancer drugs [17, 18] because its gene is over expressed in several cancers [19] and also associated with resistance towards chemotherapeutic agents [20]. Moreover, since Mcl1 has a short half-life (i.e., from ~30 minutes to a few hours), [21] inhibiting its function makes Mcl1-dependent cells more susceptible to apoptosis. Mcl1 is also structurally distinct from other anti-apoptotic proteins (e.g., Bcl-xL, Bcl-W and Bcl-2), which can be advantageous for designing selective drug molecules [11, 22].

In recent years, several experimental structures of Mcl1 have been determined in complex with different peptides [23-26] and small molecule inhibitors [27-30]. Despite these studies, the mechanistic basis of ligand binding is still poorly understood. For example, Fire *et al.* [31] demonstrated that different point mutations introduced in the pro-apoptotic Bim peptide resulted in surprisingly modest effects towards the Mcl1-Bim peptide complex stability [31]. As the crystal structures for these mutants in complex

with Mcl1 are available, thus we can investigate the mechanistic effects of the reported point mutants towards the complex stability at atomistic level using an unbinding simulation technique.

The classical molecular dynamics approach is a computationally expensive procedure to simulate the unbinding process of a bound ligand from its target molecule. To overcome this limitation, the Steered Molecular Dynamics (SMD) or Center-of-Mass (COM) pulling simulation approach has been widely used. In recent years, the SMD technique has been applied to (i) discern the actives from inactive compounds; [32] (ii) understand the dissociation pathways of different inhibitors; [33] (iii) identify hotspot regions; [34] (iv) inhibitor designing strategies; [35] (v) study the mechanical unfolding of a specific domain; [36] (vi) understand a drug resistance mechanism [37] and (vii) understand the destabilization of toxic amyloid β-peptide aggregation due to oxidation [38]. The SMD technique employs time-dependent external force (F) applied along the reaction coordinate between ligand and target protein, which acts as the initiating factor and accelerates the ligand unbinding process at a constant velocity (v) from the protein binding-pocket [39]. During the unbinding process the dynamic transition between the two states —bound and unbound— and (ii) the rupture peak force (F_{max} in pico newton, pN) required for the complete dissociation of the bound ligand can be observed. The F_{max} values obtained during the unbinding process give an estimate on the binding strength of the ligand.

In this study, we employ SMD to investigate the atomistic interactions transpiring during the unbinding process of Bim peptides from the CBG of Mcl1. In addition, we estimate the dissociation free energy (ΔG_d) using subsequent umbrella sampling (US)

simulations. The results of these simulations may give the valuable insights into rational design of selective Mcl1 inhibitors, which can be used in cancer treatment.

Material and Methods

Structure preparation. Fire *et al*. [31] reported a comprehensive study on point mutants of Bim peptide (Figure 1). The detailed investigation on the Bim mutants led us to categorize the peptides into three different groups, based on reported experimental data such as activity/binding affinity values. All group 1 and group 2 Bim peptides have been co-crystallized with Mcl1 and their structures can be retrieved from the Protein Data Bank (PDB) [40] (www.rcsb.org). The wild type Bim peptide (wt, PDB ID: 2PQK) was added in Group 1 that comprises also three different Bim mutants with measured binding affinity (K_d) values (I2dY—PDB ID: 3KJ0; I2dA — PDB ID: 3KJ1; F4aE — PDB ID: 3KJ2) [31]. Group 2 contains two mutant peptides with no reported activity/binding data: 2A (PDB ID: 3D7V) and L12Y (PDB ID: 3IO9) [10, 41]. Group 3 includes two peptide mutants with IC_{50} values: I3dF and E3gK [31]. The 3D structures of three peptides in group 3 is not available. Their coordinates were generated using the wt-Mcl1 (2PQK) structure by introducing point mutations on the Bim peptide using the Schrödinger Maestro suite (Schrödinger, LLC, New York, NY, 2019-4). These two models and the six Mcl1 co-crystals of group 1 and 2 Bim peptides from PDB were used as the starting coordinates for the MD simulations (Figure 1).
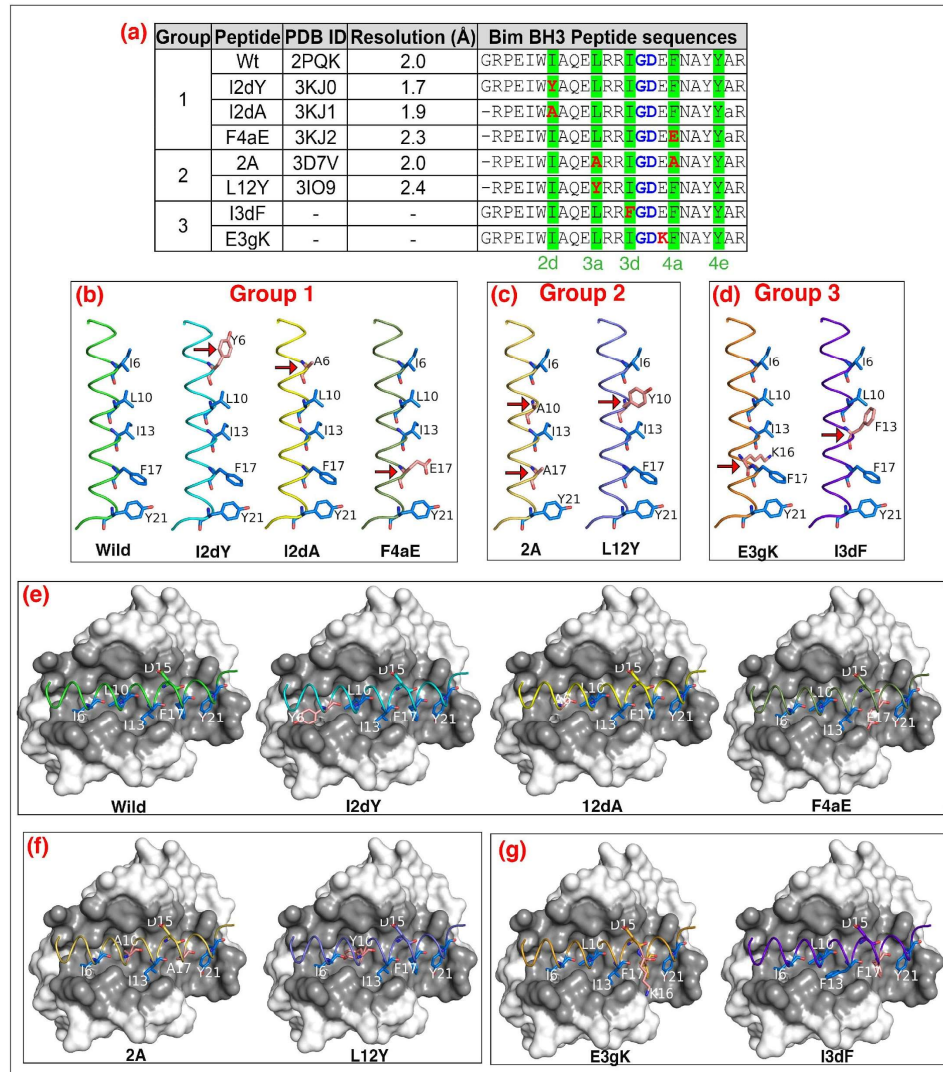
6

Figure 1: Bim peptides used in the simulations. (a) The sequences of Bim peptide. The residues involved in the point mutations (red) [31], glycine-aspartate (GD) doublet (blue) and highly conserved hydrophobic residues (green) facing the sub-pockets of Mcl1 are highlighted. (b, c and d) The α-helical representation of the Bim peptides. The mutated residues are shown in salmon sticks, indicated with red arrows and the conserved hydrophobic residues are shown in marine sticks. (e, f and g) The Bim peptides bound to the canonical binding groove (dark grey surface) of Mcl1 (white molecular surface).

Molecular Dynamics Simulations. The CHARMM27 all-atom force field embedded in the GROMACS 5.1 software package [42, 43] was used to carry out the MD simulations. Initially, all Mcl1–Bim peptide complexes were individually placed in a cubic box and solvated using the TIP3P [44] water model. The distance between the surface of the protein and the edge of the box was set to 0.9 nm. Subsequently, counter ions (Na^+ and Cl^-) were added to neutralize the systems at 0.1 M concentration. To remove initial bad contacts the simulation system was subjected to 2000 steps of all-atom energy minimization using the steepest-descent integrator. Furthermore, the system was equilibrated for 20 ns using a constant volume NVT ensemble, followed by a further equilibration using a constant pressure NPT ensemble for 10 ns. For this, the V-rescale thermostat [45] and Berendsen barostat [46] were employed, respectively. During the equilibrium steps, the default harmonic position restraints were applied on all heavy atoms present in the system. Finally, the simulation systems were subjected to a production run for 160 ns each using Parrinello-Rahman barostat [42] without any restraints. During the equilibrium and production runs, the temperature of the systems was maintained at 300 K. Bonds involving hydrogen atoms were constrained using Parallel-Linear Constraint Solver (P-LINCS) algorithm [47]. Furthermore, particle-mesh Ewald (PME) summation method [43] was used to calculate long-range electrostatic interactions. The short-range and long-range non-bonded interactions were truncated at 1.4 Å and 12 Å cut-off, respectively. The simulations were performed using a 2-fs integration time step.

Steered Molecular Dynamics. The binding strength of the complexes and the atomistic interactions transpiring during the unbinding process of Bim peptides from the CBG of

Mcl1 were investigated with the SMD technique. The average structure obtained from the last 40 ns time period (equilibrated phase of the production simulation) of the classical MD simulation, which was selected, and used as the starting structure for SMD. These protein complexes were placed in a box with dimensions of 8x8x30 Å. The current size of the box was sufficient for the total dissociation of peptides from the CBG of MCl1. Typically, in the SMD procedure the receptor protein is restrained in a fixed position, while the bound ligand is allowed to dissociate from the protein's binding pocket at a constant velocity (v). Thus, Mcl1 was restrained, and a range of constant velocities (v = 0.001 to 0.01 nm/ps) and the conventional spring constant (k = 600 kJ/mol/nm^2 $\approx$ 1020 pN/nm) [48] were applied to the COM of the Bim peptides along the z-axis. Finally, 4 ns simulation time was estimated to be sufficient to attain the complete unbinding process of the Bim peptides. Further, we carried out 4 ns SMD simulations for each complex systems. During the simulation process, the output frames were recorded at every 1 ps. The total force (F) required for the dissociation process was estimated from the output trajectories using the equation $F = k(vt - x)$, where x represents the displacement (Å) of a peptide from its initial position.

Umbrella Sampling. Subsequently, in order to estimate the free energy of dissociation (ΔG_d) of the peptides from the CBG of Mcl1 we used umbrella-sampling (US) simulations to obtain the potential of mean force (PMF) values for all the Mcl1-Bim peptide complexes. For this, a series of configuration windows were extracted along the reaction coordinate (z) from the SMD simulations. Here, the reaction coordinate is defined as the distance (Å) between the center-of-mass (COM) of the CBG of Mcl1 and the COM of the Bim peptides, each separated by 0.1 nm along the z-axis. All the selected

windows were then subjected to short 1 ns equilibration followed by 10 ns US simulations. The PMF values were estimated for the US simulations using the weighted histogram analysis (WHAM) [49] method available in GROMACS. Additionally, the error values associated with the PMF was determined using the bootstrapping method [50]. Hydrogen bonds (H-bonds) were calculated with the default distance cut-off between donor and acceptor atoms are 3.5 Å and angle cut-off of 30°. Visual inspection of every trajectory was carried out with PyMol [51] and VMD [52].

Results and Discussion

In our previous studies, we have carried out a broad range of investigations to understand the molecular mechanism of binding of the Bcl2 family proteins, especially using the MD simulation technique [53-58]. These revealed crucial details on (i) intra-molecular conformational changes of Bax protein, [53] (ii) the hotspot residues that promote heterodimerization, [55] (iii) the mechanism of small molecule inhibitors binding to Mcl1, [56] and (iv) the molecular properties involved in the complex formation of Mcl1 and small molecular inhibitors [54, 57, 58]. Based on our previous experience, the current investigation sought to understand the effects of point mutants on the complex stability at the atomistic level using an advanced MD simulation technique, such as SMD. This enhanced sampling approach accelerates the unbinding process by applying an external force to a ligand (here, Bim mutants) in the bound complex.

Classical MD Simulations. Initially, all Mcl1−peptide complexes were subjected individually to classical MD simulations for a period of 160 ns to obtain equilibrated starting structures for SMD. The results obtained from the mutants were compared with the wt peptide. The structural stability of the complexes was monitored using the root-

mean-square deviation (*rmsd*) analysis approach for the three different groups of Mcl1—

Bim peptide complexes (see Figure 2). Here, the positions of the Cα atoms of the protein-

peptide complexes over the simulation time were compared with their initial starting
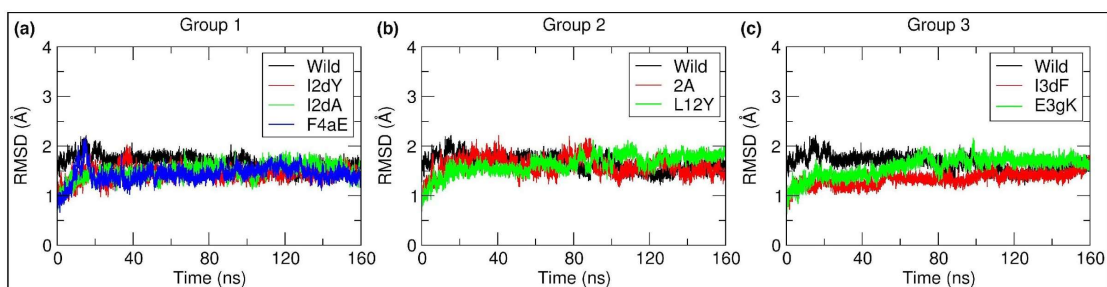
positions.

Figure 2: Root-mean-square deviation (*rmsd* in Å) of the three different groups of

Mcl1—Bim peptide complexes during the classical MD simulations (Wild = wild type).

As is clear from Figure 2, after the first 25 ns, all the complexes in group 1

converged to a stable equilibrium phase. Members in the group 2 and E3gK in group 3

showed an insignificant deviations from their initial conformation after the first 25 ns but

reached the stable equilibrium phase with the converged *rmsd* values at the later stages of

the simulations (~ around 120 ns). The equilibrated *rmsd* values were ~1.75± 0.03 Å,

1.5± 0.04 Å, 1.6±0.05 Å and 1.4±0.03 Å for group 1, 1.5±0.04 Å and 1.8±0.02 Å for

group 2, and 1.5±0.03 Å and 1.75±0.03 Å for group 3, respectively. These values suggest

that all these complexes were stable during the MD simulations. Therefore, an average

snapshot structure obtained from the last 40 ns time period of each complex was used for

the subsequent SMD investigations.

Steered Molecular Dynamics. In order to identify the appropriate force constants that

can effectively carry out the dissociation process, a series of constant velocities was

employed together with the conventional spring constant for all three groups of Mcl1—

Bim complexes (ref. Methods). Since high values of the spring constant and velocities may lead to unnatural artefacts causing complex deformities in the protein system. Therefore, these parameters were initially set to smaller values. This choice was backed up by the preliminary test simulations that failed to produce reliable outputs with higher pulling parameters (v = 0.002 to 0.01 nm/ps and spring constants > 600 kJ/mol*nm^2). Therefore, for the current investigation, the spring constant was set to 600 kJ/mol*nm^2 and the constant velocity to 0.001 nm/ps for all the complexes. In order to compare the unbinding process of multiple complexes, it is necessary to maintain the same parameters for all simulations [59]. Each unbinding simulation was carried out for a period of 4 ns.

The force-time curves were plotted for the three different groups of the Bim mutants and this plot helps to determine the maximum force that needed to disintegrate the peptide from the CBG (Figure 3). All the peptides from group 1 exhibited similar dissociation profiles at early stage inclining towards the peak and reached the peak rupture force (F_{max}) in close range to each other (stage A) (Figures 3a, 3d and Table 1).
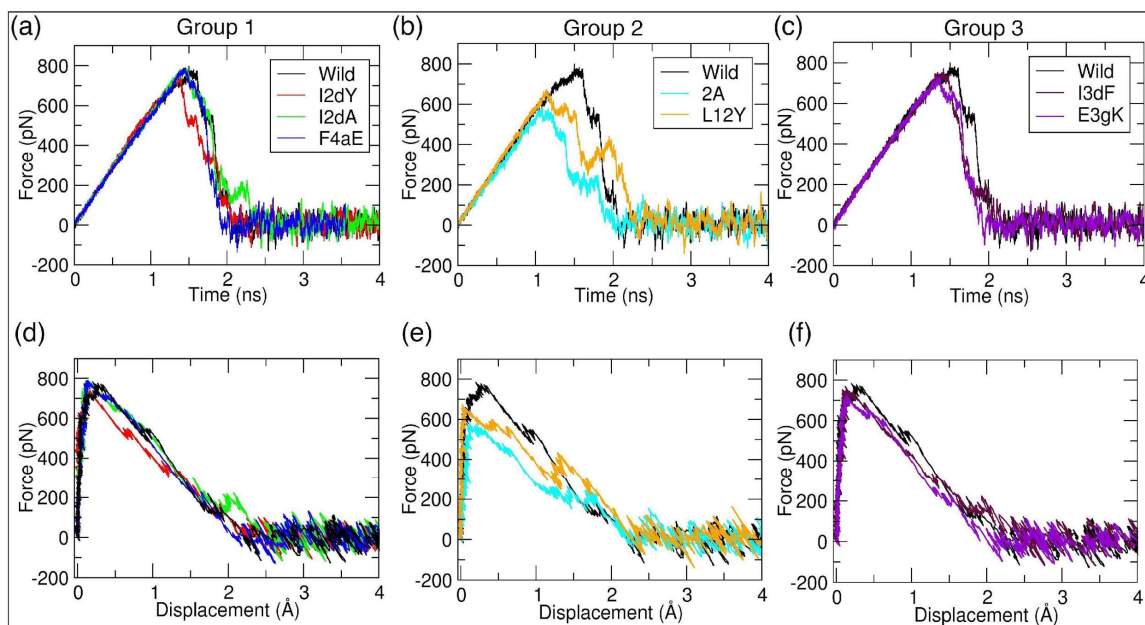
Figure 3: The force-time curve (pN) plotted against time (ns) (a - c) and displacement values (Å) (d - f) for the three groups of Bim peptides during the SMD simulation from the Mcl1 binding pocket.

Table 1: The evolution of applied external forces (F_{max} in pN) obtained for eight different Mcl1–Bim peptide complexes collected during different stages (time, ns) of the SMD simulation.

Peptide Group	Bim peptides	Stage A		Stage B		Stage C		Stage D		Stage E	
		pN	ns	pN	ns	pN	ns	pN	ns	pN	ns
1	Wt*	798	1.49	576	1.72	549	1.80	223	1.99	0	2.10
	I2dY	754	1.36	552	1.58	320	1.72	174	2.02	0	2.07
	I2dA	789	1.45	669	1.62	169	1.89	302	1.91	0	2.46
	F4aE	791	1.45	727	1.67	599	1.70	282	1.79	0	1.93
2	2A	586	1.08	446	1.36	272	1.62	248	1.80	0	2.05
	L12Y	673	1.14	605	1.37	245	1.64	438	1.94	0	2.35
3	I3dF	728	1.36	661	1.58	611	1.60	234	1.87	0	1.90
	E3gK	770	1.41	568	1.62	338	1.66	223	1.95	0	2.01

* wild type Bim peptide

The F_{max} values obtained for the group 1 peptides - wt, I2dY, I2dA and F4aE mutants were about ~798 pN, 754 pN, 789 pN, and 791 pN, respectively (Figures 4a, 5a, Supplementary figures S1a and S2a; stage A). These F_{max} values represent the force required to rupture the conserved salt-bridge between D15 of Bim and R263 of Mcl1 and a H-bond interaction between D15 of Bim and N260 of Mcl1. Subsequently, the dissociation declining from the peak occurs in a sequential manner, where only relatively weak forces are required to rupture the polar network at stage B (Figures 4b, 5b, S1b and S2b), and stage C (Figures 4c, 5c, S1c and S2c). Likewise, the force required to rupture the transient polar interactions that transpired during the unbinding process decreased further at stage D (Figures 4d, 5d, S1d and S2d). Finally, the force reached zero as the peptides completely dissociated from the Mcl1 binding groove at stage E (Figures 4e, 5e,

S1e and S2e). The similar unbinding pathways, and the close range of F_{max} peak values obtained from the SMD simulations are consistent with the literature, that explains mutations from group 1 exhibited moderate effect on complex stability [31].
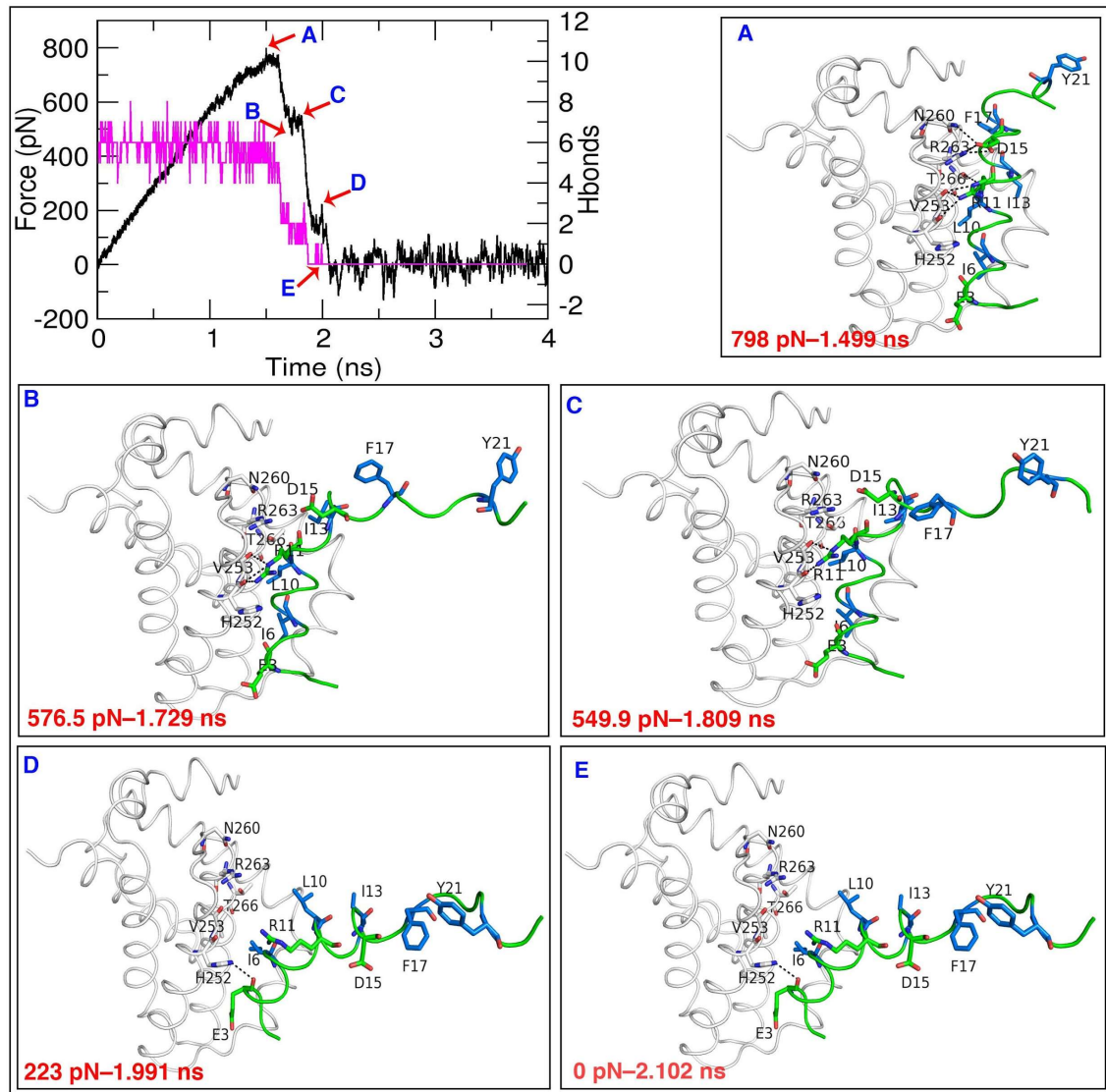

Figure 4: The force-time curve (black), and total number of H-bonds (magenta) during the 4 ns unbinding simulation for wt-Bim peptide (green) complexed with Mcl1 (white cartoon loop; PDB ID: 2PQK). The unbinding mechanism of wt–Bim was monitored through the different stages of the simulation (labeled from A to E), and the

corresponding snapshot structures of the wt-Bim−Mcl1 complex are shown with the F_{max} values at the particular time points in red. Interacting residues are shown in labelled sticks; atom color code – carbon atoms: white (Mcl1); marine (hydrophobic); green (polar); oxygen: red; nitrogen: blue. Polar interactions are shown as a black dotted line.
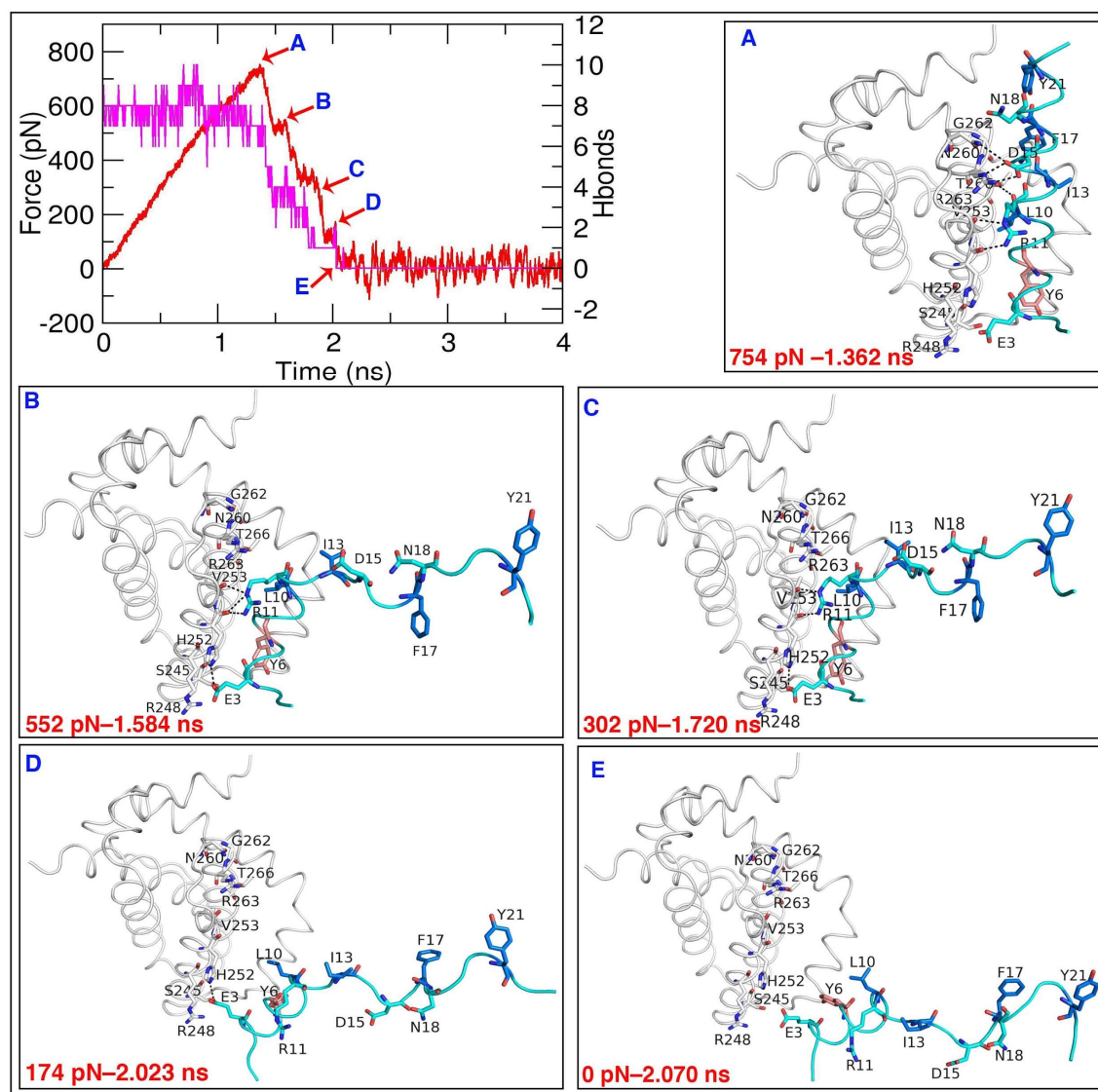

Figure 5: The force-time curve (red), and total number of H-bonds (magenta) during the 4-ns unbinding simulation for I2dY-Bim peptide (cyan) complexed with Mcl1 (white cartoon loop; PDB ID: 3KJ0). The dissociation mechanism of I2dY-Bim was monitored through the different stages of the simulation (labeled from A to E), and the corresponding snapshot

15

structures of the I2dY-Bim−Mcl1 complex are shown with the F_{max} values at the particular time points in red. Interacting residues are shown in labelled sticks; atom color code – carbon atoms: white (Mcl1); salmon (mutated); marine (hydrophobic); cyan (polar); oxygen: red; nitrogen: blue. Polar interactions are shown as a black dotted line.

The dissociation pathways obtained for peptides from group 2 are comparable to those of group 1 until the simulations reached the F_{max} peak (Figures 3b, 3e, and Table 1). The peptides from group 2 require remarkably lower rupture forces to disintegrate from the CBG of Mcl1 compared to the wt (cf. stage A). Additionally, the dissociation process of these peptides occurred in earlier stages of SMD simulations compared to wt case (at ~1.1 ns compared to wt ~1.4 ns). The F_{max} peaks for the 2A and L12Y mutants are ~586 pN and 673 pN, respectively (Figure 6a and S3a). The subsequent unbinding process exhibits similar dissociation profiles in comparison with group 1, rupturing polar contacts at stage B (Figure 6b and S3b), until the simulation reached to stage C (Figure 6c and S3c). After stage C, both peptides displayed distinct unbinding profiles. A detailed observation of the graph corresponding to mutant 2A revealed a short level force zone from stage C to D (Figure 6d) whereas the L12Y mutant's profile showed another F_{max} peak (Figure S3d). This means that the interactions at the interface region of the 2A mutant do not change significantly at the Mcl1 binding groove during that period, while the L12Y mutant requires an additional force in order to rupture the existing interactions to unbind the peptide. After stage D, both of these peptides dissociated smoothly from the CBG of Mcl1 causing F_{max} to gradually drop to zero (Figure 6e and S3e).
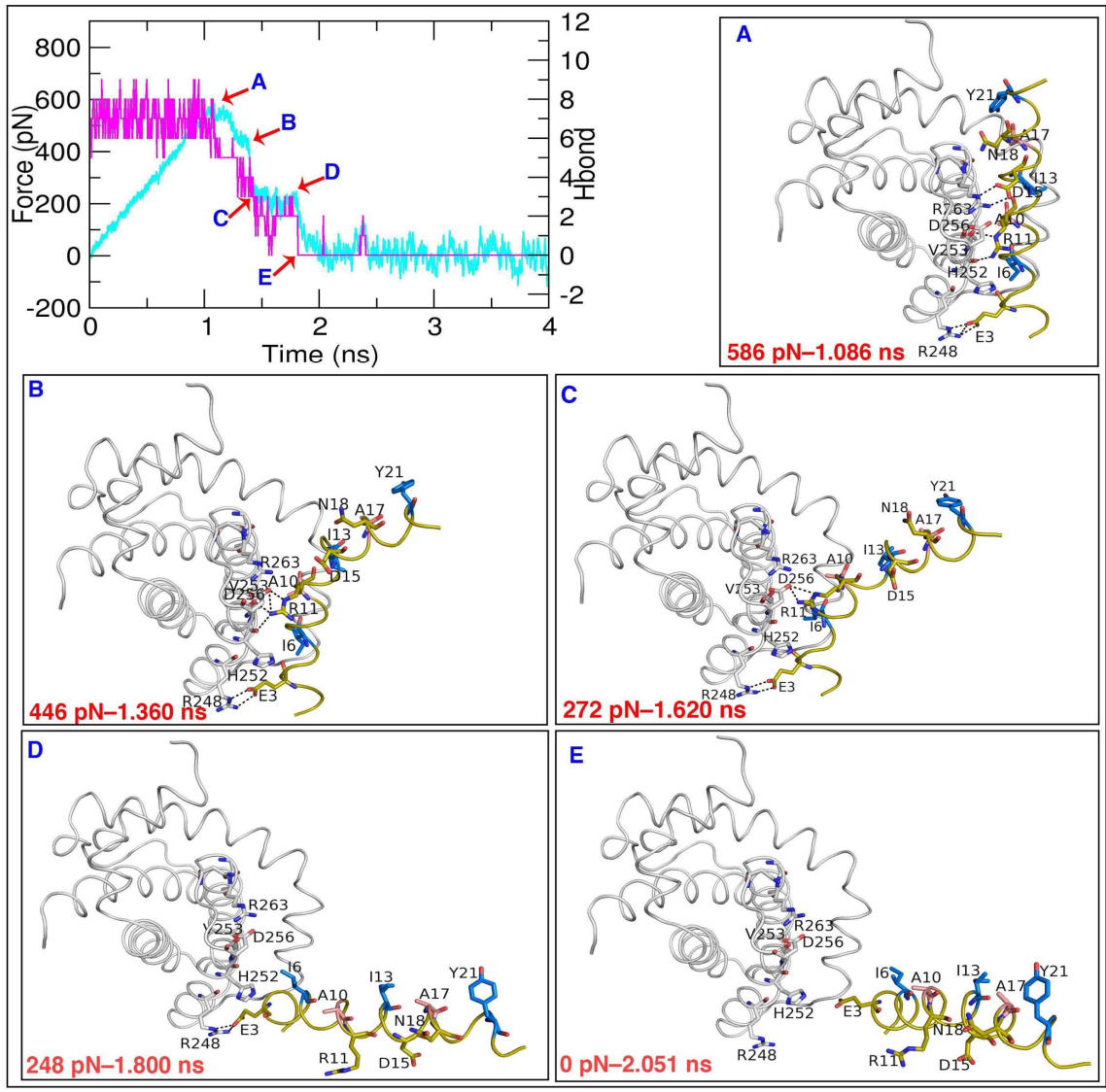
16

Figure 6: The force-time curve (cyan), and total number of H-bonds (magenta) during the 4-ns unbinding simulation for **2A**-Bim peptide (yellow) complexed with Mcl1 (white cartoon loop; PDB ID: 3D7V). The dissociation mechanism of 2A-Bim was monitored through the different stages of the simulation (labeled from A to E), and the corresponding snapshot structures of the 2A-Bim−Mcl1 complex are shown with the F_{max} values at the particular time points in red. Interacting residues are shown in labelled sticks; atom color code – carbon atoms: white (Mcl1); salmon (mutated); marine (hydrophobic); yellow (polar); oxygen: red; nitrogen: blue. Polar interactions are shown as a black dotted line.

17

The dissociation pathways and displacement values obtained for the I3dF and E3gK peptides from group 3 exhibited the unbinding profile similar to wt. However, the F_{max} peak forces obtained are somewhat lower compared to wt (Figures 3c, 3f and Table 1). Also, the peptides initiated the disintegration process only slightly before (~ 1.45 ns) than the wt (~ 1.5 ns). The maximum F_{max} obtained for the I3dF and E3gK mutants is ~770 pN and ~728 pN, respectively (Figure 7a and S4a). This peak force ruptures the conserved polar contacts between the peptides and the Mcl1 binding groove, similar to the simulations of the other two groups. The lower force is required in the subsequent dissociation process, where small peaks are observed during the group 3 mutant's dissociation at stages B to D (Figures 7b-d and S4b-d). Finally, both of these peptides completely dissociated from the Mcl1 binding groove at stage E (Figure 7e and S4e). Overall, it was observed that all Bim peptides were completely dissociated from the Mcl1 binding groove at around ~2.5 ns SMD simulations.
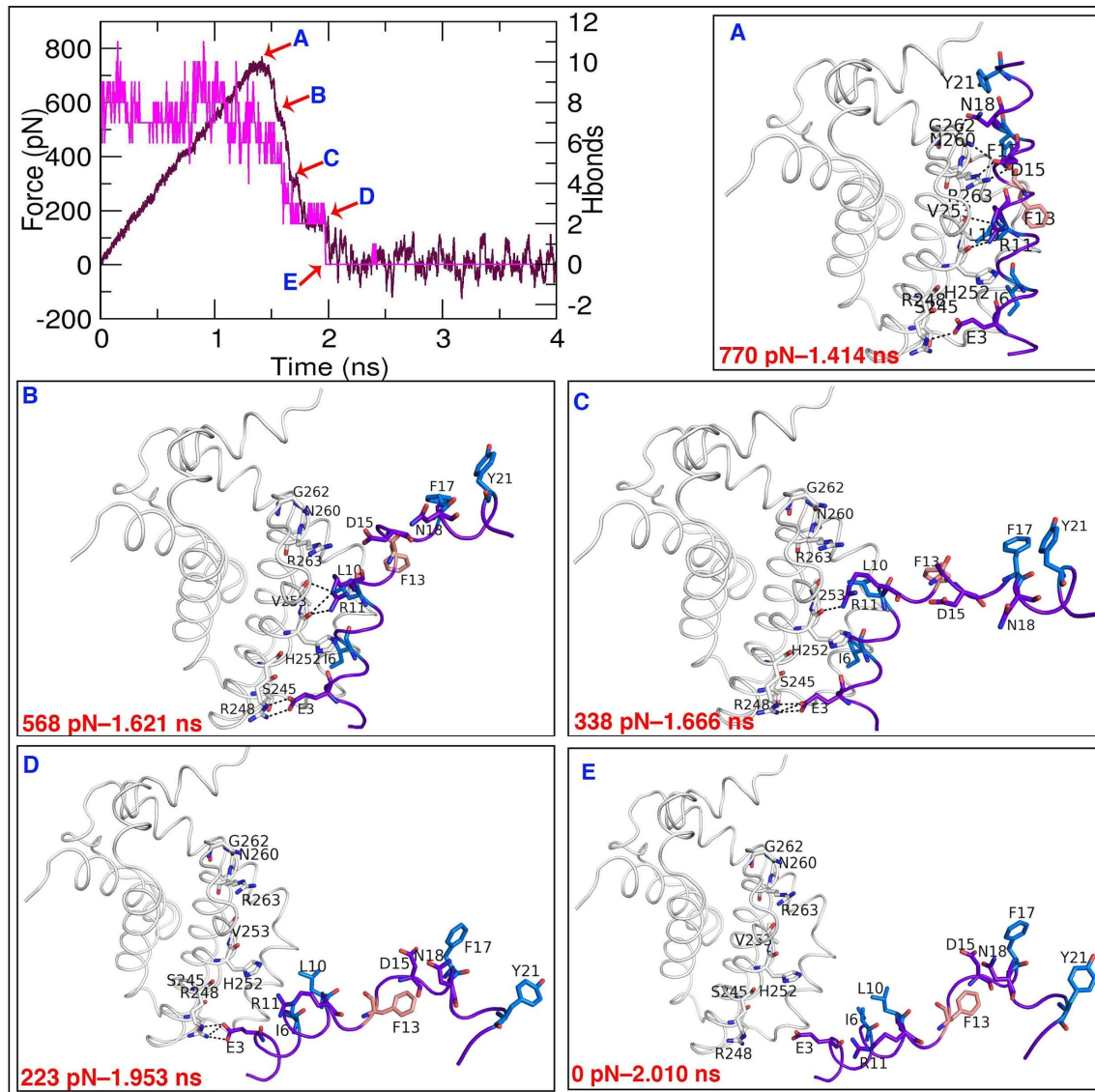
Figure 7: The force-time curve (maroon), and total number of H-bonds (magenta) during the 4-ns unbinding simulation for I3dF-Bim peptide (purple) complexed with Mcl1 (white cartoon loop). The dissociation mechanism of I3dF-Bim was monitored through the different stages of the simulation (labeled from A to E), and the corresponding snapshot structures of the I3dF-Bim−Mcl1 complex are shown with the F_{max} values at the particular time points in red. Interacting residues are shown in labelled sticks; atom color code – carbon atoms: white (Mcl1); salmon (mutated); marine (hydrophobic); purple

(polar); oxygen: red; nitrogen: blue. Polar interactions are shown as a black dotted line.

It has been observed that when the leucine present at the 3a position (sub pocket 2 – P2) of the PA peptides is mutated to alanine, it significantly affects the specificity and binding to the CBG of Mcl1 [10]. The effect of mutations at this specific position was clearly observed in our SMD simulations. Particularly, the 2A mutant with an alanine at 3a and 4a positions showed a remarkable drop in the F_{max} value (from ~798 pN of the wt to ~586 pN), and a distinct dissociation pathway in comparison with the wt. Similarly, the L12Y mutant with a tyrosine residue at 3a position exhibited a distinct unbinding pathway showing the lower F_{max} value (~673 pN) compared to the wt including the second F_{max} peak. Other mutations in the peptides of group 1 and 3 were located elsewhere than at the 3a position exhibited only slight differences in the dissociation pathways according to the force-time curves.

Mechanistic insights into the dissociation of Bim peptides from the CBG of Mcl1

To understand the mechanistic basis of the peptide dissociation from the CBG of Mcl1, the binding interface was monitored for the changes in the number of polar contacts in detail. The peak force obtained from the SMD simulation denotes the maximum force required to rupture the polar contacts at the interface region. Therefore, the changes in the number of hydrogen bonds between the Bim mutants and the Mcl1 groove were calculated and plotted in comparison with the wt (see Figure 8). The wt peptide exhibited ~6 H-bonds in the beginning of the simulation (t=0 ns), while the mutants showed even up to 12 H-bonds. Subsequently, the number of H-bonds gradually decreased over the time and reached zero at complete dissociation stage. In order to investigate the peptide dissociation mechanism in detail, the atomic coordinates

corresponding to the F_{max} peak values (labelled from A to E in Figures 4-7 and S1-S4) were visually investigated.
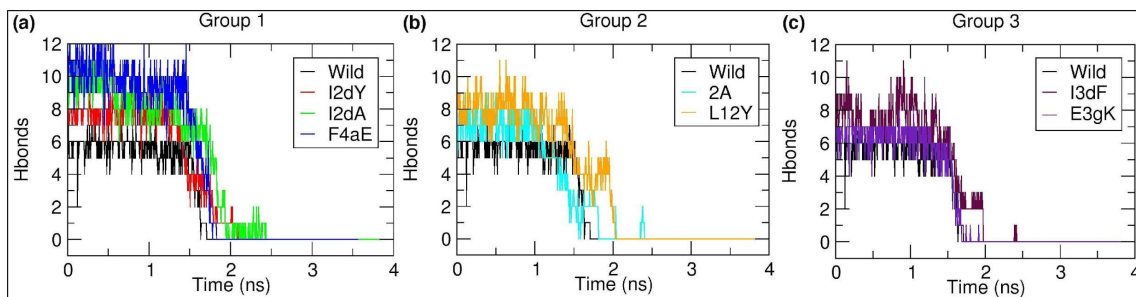

Figure 8: The number of hydrogen bonds during the unbinding process of the three different groups of peptides from the CBG of Mcl1 over time.

Several studies have demonstrated that the conserved polar interaction network— (i) a salt-bridge interaction between D15 of the Bim peptide and R263 of Mcl1, and (ii) a hydrogen bond interaction of D15 with N260 of Mcl1—plays a major role in complex stability.[60, 61] Therefore, it is essential to investigate the role of this specific polar network during the unbinding process for all the peptide complexes at stage A (Figures 4a-7a and S1a-S4a). The SMD investigation confirms that this polar interaction network is strong and remains stable for a long period (more than 1 ns) during the simulation by delaying the initiation of the unbinding process. As a result, the peptides require the maximum force (F_{max}) to disrupt these conserved polar interactions before being completely released from the CBG. Initially, the hydrogen bond between the side chain carboxylate of D15 of the peptide and the side chain amide of N260 of Mcl1 was disrupted. In the next stage, the strong salt bridge interaction between the side chain carboxylate of D15 of the peptide and the side chain guanidium of R263 of Mcl1 was disrupted in all the complexes. The unbinding process of peptides from groups 1 and 3

occurred approximately at the same time interval (between 1.3 ns to 1.4 ns). Also, the maximum rupture forces (F_{max}) are in the same range (group 1: ~798 pN, ~754 pN, ~789 pN and ~791 pN, and group 3: ~728 pN and ~770 pN). Furthermore, the F_{max} values for the group 3 peptides obtained in our simulations follow the same order of the experimental (IC_{50}) values [31]. In contrast, peptides in group 2 initiated the disintegration process slightly earlier time period (~ between 1.0 and 1.1 ns). The F_{max} values for the peptides from the group 2 are significantly lower (~586 pN and ~673 pN), which resulted in an early release of the peptides from the binding groove. In this case, the mutations destabilize the internal hydrophobic interactions that are crucial for the strong binding. The results from the group 2 peptides were also in agreement with the previous reports that highlight the importance of the residue at the 3a position. The point mutation at this position would cause a significant drop in the binding affinity [10]. Thus, our SMD simulations also confirmed the critical role of the conserved polar network for binding of peptide to the CBG of Mcl1. It eventually determines the residence time and the maximum F_{max} values required for the peptide dissociation process, although mutations at position 2a may significantly affect these values.

At stage B of the unbinding process (Figures 4b-7b and S1b-S4b), the occurrence of dissociation was delayed due to three polar contacts. The side chain guanidium group of R11 of the peptide formed two H-bonds with the backbone oxygen atom of H252, and a single H-bond with the backbone oxygen atom of V253 of Mcl1. Particularly, a salt bridge interaction between the side chain guanidium of R11, and the side chain carboxyl group of D256 of Mcl1 was also observed in alanine mutated peptides (I2dA of group 1; and 2A and L12Y of group 2). This salt bridge interaction is most likely formed to

replace the weak interactions caused by the mutation. In order to disrupt these polar networks, generally a small rupture force was required when compared with the rupture force needed to break the conserved polar contacts (Table 1) (in the range of 446 pN and 727 pN). However, only one H-bond between the backbone oxygen atom of H252 and the NE atom of the side chain guanidium group of R11 was disrupted, while the salt bridge between the side chain guanidium of R11, and the side chain carboxyl group of D256 of Mcl1 remained intact resulting in only a slight dissociation of the peptides from CBG of Mcl1.

Rapidly, the simulation reached stage C during which the F_{max} required to disrupt the next polar contacts was within the range between 169 pN and 611 pN (Figures 4c-7c and S1c-S4c, Table 1). At this stage, all other peptides required moderate F_{max} —320 pN to 611 pN— but for the alanine mutants lower F_{max} —169 pN to 272 pN was enough to induce the dissociation process. The outward movement of the peptides disrupted the polar network between the side chain guanidium of R11 and the backbone oxygen atoms of H252 and V253 of Mcl1, in most of the cases. Disruption of this polar network occurred in a stepwise manner, and the simulation reached stage D, where a major part of the peptide dissociated from the CBG.

At stage D, the complex remained intact with a charged interaction between the carboxylate side chain of E3 of the peptide and the guanidium side chain of R248 of Mcl1 in most of the cases (Figures 4d-7d, and S1d-S4d). In wt, the side chain imidazole group of H252 of Mcl1 forms a transient polar interaction with the backbone oxygen and the side chain carboxylate of E3 in I2dY and E3gK peptides. Interestingly, the tyrosine replaced by the leucine in the L12Y peptide forms a transient H-bond with the side chain

oxygen of T267 of Mcl1. Due to this, the R11 residue of the peptide moved towards to the binding pocket and established a stronger ionic interaction with D256 and also a transient H-bond interaction with the backbone oxygen of H252 of Mcl1. Thus, the force required to disrupt these new polar networks for L12Y raised up to 438 pN (see Table 1). In general, for the other peptides, the F_{max} was significantly lower (from 174 pN to 282 pN). Eventually, the simulation reached to the stage E (Figures 4e-7e and S1e-S4e), where the F_{max} reached 0 pN and the peptides were completely dissociated from the CBG.

Thus, our SMD simulations shed light on the possible mechanistic effects of the reported mutations and the crucial residues involved in binding the peptides in the CBG of Mcl1. The analysis of simulation trajectories revealed that he dissociation process was initiated from the C-terminal in all peptides despite applying the external force to their COM.

Potential of Mean Force (PMF) estimation from the unbinding simulations

The calculation of the PMF profile during the peptide dissociation process predicts the dissociation free energy (ΔG_d), i.e., energy difference between the Bim peptide in the bound and unbound state. To obtain the PMF profiles, (US) simulations were carried out using a series of initial configurations of Mcl1−Bim peptide complexes obtained from the SMD outputs (see Figure 9).
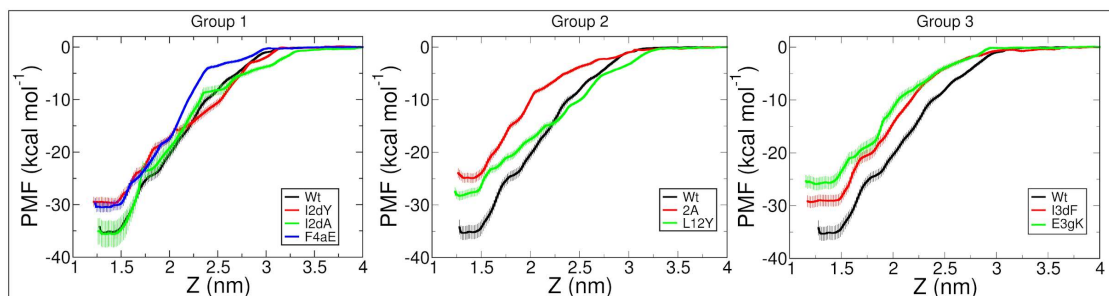
Figure 9: The dissociation free energy (ΔG_d) profiles (PMF curves) calculated using the reaction coordinates (z) obtained from the SMD simulations. The z is defined as the distance between the COM of the CBG of Mcl1 and the Bim peptides, each separated by 0.1 nm windows along the *z*-axis. The error associated with PMF is given in pale colour.

Although all the peptides from the three groups displayed very similar dissociation profiles (see Figure 3), the ΔG_d values (see Figure 9 and Table 2) showed significant differences. In general, the mutants from group 1 exhibited PMF profiles resembling the wt. On the other hand, the mutants from the group 2 and 3 showed larger differences in comparison with the wt-Bim. Thus, the ΔG_d values obtained for the group 1 peptides are mostly closer to the wt than the ΔG_d values of the peptides in the other groups. For example, the ΔG_d value for the I2dA mutant exhibits similar energy profile in comparison with wt, while the ΔG_d of I2dY and F4aE peptides shows only a slight difference. In addition, these mutants do not exhibit much difference in binding affinity. Whereas, the peptides from group 2 (2A; -28.27 kcal/mol) and 3 (E3gK; -25.92 kcal/mol) shows clear differences in its free energy profiles. This result shows that these mutations can drastically affect the binding affinity.

Table 2: Binding free energies (ΔG_d) for each Mcl1–BH3 peptide complex obtained from the US simulations. The experimental values were obtained from the literature [31].

Peptide Group	Peptide	kcal/mol		Experimental values
		ΔG_d	ΔG_{exp} [a]	IC_{50} / K_d* (nM)
1	Wt[b]	-35.32	-13.78	14.0±0.9
	I2dY	-29.70	-NA-[c]	<2*
	I2dA	-35.62	-NA-	<2*
	F4aE	-32.51	-NA-	<2*
2	2A	-28.27	-NA-	-ND-[d]
	L12Y	-29.93	-NA-	-ND-
3	I3dF	-29.34	-14.60	56.2±9.3
	E3gK	-25.92	-14.90	92.7±8.9

[a] The experimental binding free energies (ΔG_{exp}) were converted from the IC_{50} values using $-RT \ln(IC_{50})$; [b] wt = wild type; [c] NA = not applicable; [d] ND = not determined

Furthermore, a detailed investigation of the PMF profiles revealed that all the peptides in group 1 completely dissociated from the CBG of the Mcl1 at ~3.3 Å distance, while the group 2 and 3 PMF profiles showed a complete dissociation at the distances of ~3.25 Å and ~3 Å, respectively. The reason behind this might be due to the group 1 mutants require higher energies to dissociate along the reaction coordinate, while the mutants from group 2 and 3 require less energy in comparison with the wt.

Conclusion

In the present study, mechanistic effects of point mutations on pro-apoptotic Bim peptides binding to the CBG of Mcl1 were investigated using atomistic level SMD

simulations. The mechanistic insights from the dissociation pathways of the peptides from the CBG of Mcl1 provide understanding on how the mutation introduced in the peptides at 3a position causes significantly low F_{max} value (< 675 pN) (and thus reduces the binding affinity), whereas the rest of the mutants need higher F_{max} value (> 725 pN), comparable to the wt peptide. Particularly, the investigation results revealed that the unbinding process of the peptides occurred by rupturing the polar contacts at the binding interface in a step-wise manner. Noticeably, F_{max} reached its highest value when disrupting the conserved polar interaction network between D15 of the peptide and N260 and R263 of Mcl1, in all cases. The distance analysis between the mutated peptide residues and COM of the interacting residues of Mcl1 reveals that the mutations at 3a and 4a positions caused the peptides to dissociate from the CBG of Mcl1 at the earlier stages of the simulation than the mutations at other positions. Moreover, we carried out the US simulation for the SMD outputs to predict the dissociation free energy for all the studied complexes. The obtained free energy profiles help to understand the effects of the mutations complexes along the reaction coordinate. Overall, the current investigation demonstrates that the mutants I2dA and F4aE reflect similar binding energies, while the mutants 2A and L12Y show significant decrease in binding energies in comparison with wt. Our study may provide valuable insights into the design of novel Bim like peptide inhibitors to downregulate Mcl1 function that is crucial in cancer treatment. In general, our investigation results might assist pharmacological community to design targeted inhibitors for manipulation of Mcl1 function.

Acknowledgements

ORCID

Parthiban Marimuthu: 0000-0003-4960-2160

Jamoliddin Razzokov: 0000-0002-3098-0797

References

[1] P.E. Czabotar, G. Lessene, A. Strasser, J.M. Adams, Control of apoptosis by the BCL-2 protein family: implications for physiology and therapy, Nat Rev Mol Cell Biol 15(1) (2014) 49-63.

[2] F. Edlich, BCL-2 proteins and apoptosis: Recent insights and unknowns, Biochem Biophys Res Commun 500(1) (2018) 26-34.

[3] T. Moldoveanu, Q. Liu, A. Tocilj, M. Watson, G. Shore, K. Gehring, The X-ray structure of a BAK homodimer reveals an inhibitory zinc binding site, Molecular cell 24(5) (2006) 677-688.

[4] S. Thomas, B.A. Quinn, S.K. Das, R. Dash, L. Emdad, S. Dasgupta, X.Y. Wang, P. Dent, J.C. Reed, M. Pellecchia, D. Sarkar, P.B. Fisher, Targeting the Bcl-2 family for cancer therapy, Expert Opin Ther Targets 17(1) (2013) 61-75.

[5] P.E. Czabotar, E.F. Lee, M.F. van Delft, C.L. Day, B.J. Smith, D.C. Huang, W.D. Fairlie, M.G. Hinds, P.M. Colman, Structural insights into the degradation of Mcl-1 induced by BH3 domains, Proc Natl Acad Sci U S A 104(15) (2007) 6217-6222.

[6] C.L. Day, C. Smits, F.C. Fan, E.F. Lee, W.D. Fairlie, M.G. Hinds, Structure of the BH3 domains from the p53-inducible BH3-only proteins Noxa and Puma in complex with Mcl-1, J Mol Biol 380(5) (2008) 958-71.

[7] C. Smits, P.E. Czabotar, M.G. Hinds, C.L. Day, Structural plasticity underpins promiscuous binding of the prosurvival protein A1, Structure 16(5) (2008) 818-829.

[8] E. Gavathiotis, M. Suzuki, M.L. Davis, K. Pitter, G.H. Bird, S.G. Katz, H.C. Tu, H. Kim, E.H. Cheng, N. Tjandra, L.D. Walensky, BAX activation is initiated at a novel interaction site, Nature 455(7216) (2008) 1076-81.

[9] P.S. Jeng, A. Inoue-Yamauchi, J.J. Hsieh, E.H. Cheng, BH3-Dependent and Independent Activation of BAX and BAK in Mitochondrial Apoptosis, Current opinion in physiology 3 (2018) 71-81.

[10] E.F. Lee, P.E. Czabotar, M.F. van Delft, E.M. Michalak, M.J. Boyle, S.N. Willis, H. Puthalakath, P. Bouillet, P.M. Colman, D.C. Huang, W.D. Fairlie, A novel BH3 ligand that selectively targets Mcl-1 reveals that apoptosis can proceed without Mcl-1 degradation, J Cell Biol 180(2) (2008) 341-55.

[11] E.F. Lee, P.E. Czabotar, B.J. Smith, K. Deshayes, K. Zobel, P.M. Colman, W.D. Fairlie, Crystal structure of ABT-737 complexed with Bcl-xL: implications for selectivity of antagonists of the Bcl-2 family, Cell death and differentiation 14(9) (2007) 1711-1719.

[12] W.J. Placzek, M. Sturlese, B. Wu, J.F. Cellitti, J. Wei, M. Pellecchia, Identification of a novel Mcl-1 protein binding motif, J Biol Chem 286(46) (2011) 39829-39835.

[13] J. Chen, H. Zhou, A. Aguilar, L. Liu, L. Bai, D. McEachern, C.Y. Yang, J.L. Meagher, J.A. Stuckey, S. Wang, Structure-based discovery of BM-957 as a potent small-molecule inhibitor of Bcl-2 and Bcl-xL capable of achieving complete tumor regression, J Med Chem 55(19) (2012) 8502-14.

[14] S. Dutta, S. Gulla, T.S. Chen, E. Fire, R.A. Grant, A.E. Keating, Determinants of BH3 binding specificity for Mcl-1 versus Bcl-xL, J Mol Biol 398(5) (2010) 747-62.

[15] L. Chen, S.N. Willis, A. Wei, B.J. Smith, J.I. Fletcher, M.G. Hinds, P.M. Colman, C.L. Day, J.M. Adams, D.C. Huang, Differential targeting of prosurvival Bcl-2 proteins by their BH3-only ligands allows complementary apoptotic function, Molecular cell 17(3) (2005) 393-403.

[16] T. Kuwana, L. Bouchier-Hayes, J.E. Chipuk, C. Bonzon, B.A. Sullivan, D.R. Green, D.D. Newmeyer, BH3 domains of BH3-only proteins differentially regulate Bax-mediated mitochondrial membrane permeabilization both directly and indirectly, Molecular cell 17(4) (2005) 525-35.

[17] W. Xiang, C.Y. Yang, L. Bai, MCL-1 inhibition in cancer treatment, OncoTargets and therapy 11 (2018) 7301-7314.

[18] A.C. Timucin, H. Basaga, O. Kutuk, Selective targeting of antiapoptotic BCL-2 proteins in cancer, Medicinal research reviews 39(1) (2019) 146-175.

[19] R. Yamaguchi, L. Lartigue, G. Perkins, Targeting Mcl-1 and other Bcl-2 family member proteins in cancer therapy, Pharmacology & therapeutics (2018).

[20] E. Wesarg, S. Hoffarth, R. Wiewrodt, M. Kroll, S. Biesterfeld, C. Huber, M. Schuler, Targeting BCL-2 family proteins to overcome drug resistance in non-small cell lung cancer, International journal of cancer. Journal international du cancer 121(11) (2007) 2387-94.

[21] J. Zhuang, H.J. Brady, Emerging role of Mcl-1 in actively counteracting BH3-only proteins in apoptosis, Cell death and differentiation 13(8) (2006) 1263-7.

[22] T. Oltersdorf, S.W. Elmore, A.R. Shoemaker, R.C. Armstrong, D.J. Augeri, B.A. Belli, M. Bruncko, T.L. Deckwerth, J. Dinges, P.J. Hajduk, M.K. Joseph, S. Kitada, S.J. Korsmeyer, A.R. Kunzer, A. Letai, C. Li, M.J. Mitten, D.G. Nettesheim, S. Ng, P.M. Nimmer, J.M. O'Connor, A. Oleksijew, A.M. Petros, J.C. Reed, W. Shen, S.K. Tahir, C.B. Thompson, K.J. Tomaselli, B. Wang, M.D. Wendt, H. Zhang, S.W. Fesik, S.H. Rosenberg, An inhibitor of Bcl-2 family proteins induces regression of solid tumours, Nature 435(7042) (2005) 677-81.

[23] G.W. Foight, J.A. Ryan, S.V. Gulla, A. Letai, A.E. Keating, Designed BH3 Peptides with High Affinity and Specificity for Targeting Mcl-1 in Cells, ACS chemical biology 9(9) (2014) 1962-1968.

[24] J.M. Brouwer, P. Lan, A.D. Cowan, J.P. Bernardini, R.W. Birkinshaw, M.F. van Delft, B.E. Sleebs, A.Y. Robin, A. Wardak, I.K. Tan, B. Reljic, E.F. Lee, W.D. Fairlie, M.J. Call, B.J. Smith, G. Dewson, G. Lessene, P.M. Colman, P.E. Czabotar, Conversion of Bim-BH3 from Activator to Inhibitor of Bak through Structure-Based Design, Molecular cell 68(4) (2017) 659-672 e9.

[25] D.d.A. A, J. Lim, K.C. Wu, Y. Xiang, A.C. Good, R. Skerlj, D.P. Fairlie, Bicyclic Helical Peptides as Dual Inhibitors Selective for Bcl2A1 and Mcl-1 Proteins, J Med Chem 61(7) (2018) 2962-2972.

[26] R. Rezaei Araghi, G.H. Bird, J.A. Ryan, J.M. Jenson, M. Godes, J.R. Pritz, R.A. Grant, A. Letai, L.D. Walensky, A.E. Keating, Iterative optimization yields Mcl-1-targeting stapled peptides with selective cytotoxicity to Mcl-1-dependent cancer cells, Proc Natl Acad Sci U S A 115(5) (2018) E886-E895.

[27] Z. Wang, W. Xu, T. Song, Z. Guo, L. Liu, Y. Fan, A. Wang, Z. Zhang, Fragment-Based Design, Synthesis, and Biological Evaluation of 1-Substituted-indole-2-carboxylic Acids as Selective Mcl-1 Inhibitors, Arch Pharm (Weinheim) 350(1) (2017).

[28] S. Shaw, Z. Bian, B. Zhao, J.C. Tarr, N. Veerasamy, K.O. Jeon, J. Belmar, A.L. Arnold, S.A. Fogarty, E. Perry, J.L. Sensintaffar, D.V. Camper, O.W. Rossanese, T. Lee, E.T. Olejniczak, S.W. Fesik, Optimization of Potent and Selective Tricyclic Indole Diazepinone Myeloid Cell Leukemia-1 Inhibitors Using Structure-Based Design, J Med Chem 61(6) (2018) 2410-2421.

[29] A.E. Tron, M.A. Belmonte, A. Adam, B.M. Aquila, L.H. Boise, E. Chiarparin, J. Cidado, K.J. Embrey, E. Gangl, F.D. Gibbons, G.P. Gregory, D. Hargreaves, J.A. Hendricks, J.W. Johannes, R.W. Johnstone, S.L. Kazmirski, J.G. Kettle, M.L. Lamb, S.M. Matulis, A.K. Nooka, M.J. Packer, B. Peng, P.B. Rawlins, D.W. Robbins, A.G. Schuller, N. Su, W. Yang, Q. Ye, X. Zheng, J.P. Secrist, E.A. Clark, D.M. Wilson, S.E. Fawell, A.W. Hird, Discovery of Mcl-1-specific inhibitor AZD5991 and preclinical activity in multiple myeloma and acute myeloid leukemia, Nat Commun 9(1) (2018) 5341.

[30] Y. Wan, N. Dai, Z. Tang, H. Fang, Small-molecule Mcl-1 inhibitors: Emerging anti-tumor agents, Eur J Med Chem 146 (2018) 471-482.

[31] E. Fire, S.V. Gulla, R.A. Grant, A.E. Keating, Mcl-1-Bim complexes accommodate surprising point mutations via minor structural changes, Protein Sci 19(3) (2010) 507-519.

[32] J.S. Patel, A. Berteotti, S. Ronsisvalle, W. Rocchia, A. Cavalli, Steered molecular dynamics simulations for studying protein-ligand interaction in cyclin-dependent kinase 5, J Chem Inf Model 54(2) (2014) 470-80.

[33] A.M. Capelli, G. Costantino, Unbinding pathways of VEGFR2 inhibitors revealed by steered molecular dynamics, J Chem Inf Model 54(11) (2014) 3124-36.

[34] M. Ylilauri, O.T. Pentikainen, MMGBSA as a tool to understand the binding affinities of filamin-peptide interactions, J Chem Inf Model 53(10) (2013) 2626-2633.

[35] J. Lesitha Jeeva Kumari, R. Jesu Jaya Sudan, C. Sudandiradoss, Evaluation of peptide designing strategy against subunit reassociation in mucin 1: A steered molecular dynamics approach, PLoS One 12(8) (2017) e0183041.

[36] V.V. Mykuliak, A.W.M. Haining, M. von Essen, A. Del Rio Hernandez, V.P. Hytonen, Mechanical unfolding reveals stable 3-helix intermediates in talin and alpha-catenin, PLoS Comput Biol 14(4) (2018) e1006126.

[37] D. Pan, W. Xue, W. Zhang, H. Liu, X. Yao, Understanding the drug resistance mechanism of hepatitis C virus NS3/4A to ITMN-191 due to R155K, A156V, D168A/E mutations: a computational study, Biochim Biophys Acta 1820(10) (2012) 1526-34.

[38] J. Razzokov, M. Yusupov, A. Bogaerts, Oxidation destabilizes toxic amyloid beta peptide aggregation, Scientific reports 9(1) (2019) 5476.

[39] J.C. Phillips, R. Braun, W. Wang, J. Gumbart, E. Tajkhorshid, E. Villa, C. Chipot, R.D. Skeel, L. Kale, K. Schulten, Scalable molecular dynamics with NAMD, J Comput Chem 26(16) (2005) 1781-1802.

[40] H. Berman, K. Henrick, H. Nakamura, J.L. Markley, The worldwide Protein Data Bank (wwPDB): ensuring a single, uniform archive of PDB data, Nucleic Acids Res 35(Database issue) (2007) D301-3.

[41] E.F. Lee, P.E. Czabotar, H. Yang, B.E. Sleebs, G. Lessene, P.M. Colman, B.J. Smith, W.D. Fairlie, Conformational changes in Bcl-2 pro-survival proteins determine their capacity to bind ligands, J Biol Chem 284(44) (2009) 30508-17.

[42] M. Parrinello, A. Rahman, Polymorphic transitions in single crystals: A new molecular dynamics method, J. Appl. Phys. 52 (1981) 7182-7190.

[43] T. Darden, D. York, L. Pedersen, Particle Mesh Ewald - an N.Log(N) Method for Ewald Sums in Large Systems, J. Chem. Phys. 98(12) (1993) 10089-10092.

[44] M.W.J. Mahoney, W. L., A five-site model for liquid water and the reproduction of the density anomaly by rigid, nonpolarizable potential functions, J. Chem. Phys 112(20) (2000) 8910-8922.

[45] G. Bussi, D. Donadio, M. Parrinello, Canonical sampling through velocity rescaling, J Chem Phys 126(1) (2007) 014101.

[46] H.J.C. Berendsen, J.P.M. Postma, W.F. van Gunsteren, A. DiNola, J.R. Haak, Molecular dynamics with coupling to an external bath., J Chem Phys 81 (1984) 3684–3690.

[47] B. Hess, P-LINCS: A parallel linear constraint solver for molecular simulation, J Chem Theory Comput 4(1) (2008) 116-122.

[48] B.K. Mai, M.S. Li, Neuraminidase inhibitor R-125489--a promising drug for treating influenza virus: steered molecular dynamics approach, Biochem Biophys Res Commun 410(3) (2011) 688-91.

[49] S. Kumar, Rosenberg, J. M., Bouzida, D., Swendsen, R. H. Kollman, P. A., The weighted histogram analysis method for free-energy calculations on biomolecules. I. The method., J Comput Chem 13 (1992) 1011-1021.

[50] J.S. Hub, B.L. de Groot, Does CO2 permeate through aquaporin-1?, Biophys J 91(3) (2006) 842-8.

[51] W.L. DeLano, Pymol: An open-source molecular graphics tool, CCP4 Newsletter on protein crystallography 40(4) (2002) 82-92.

[52] W. Humphrey, A. Dalke, K. Schulten, VMD: visual molecular dynamics, J Mol Graph 14(1) (1996) 33-8, 27-8.

[53] C. Koshy, M. Parthiban, R. Sowdhamini, 100 ns molecular dynamics simulations to study intramolecular conformational changes in Bax, J Biomol Struct Dyn 28(1) (2010) 71-83.

[54] P. Marimuthu, P.K. Balasubramanian, K. Singaravelu, Deciphering the crucial molecular properties of a series of Benzothiazole Hydrazone inhibitors that targets anti-apoptotic Bcl-xL protein, J Biomol Struct Dyn (2017) 1-14.

[55] P. Marimuthu, K. Singaravelu, Deciphering the crucial residues involved in heterodimerization of Bak peptide and anti-apoptotic proteins for apoptosis, J Biomol Struct Dyn (2017) 1-12.

[56] P. Marimuthu, K. Singaravelu, Prediction of Hot Spots at Myeloid Cell Leukemia-1-Inhibitors Interface using Energy Estimation and Alanine Scanning Mutagenesis, Biochemistry (2018).

[57] P. Marimuthu, K. Singaravelu, Unraveling the Molecular Mechanism of Benzothiophene and Benzofuran scaffold merged compounds binding to anti-apoptotic Myeloid cell leukemia 1, J Biomol Struct Dyn (2018) 1-49.

[58] K. Singaravelu, P.K. Balasubramanian, P. Marimuthu, Investigating the Molecular Basis of N-Substituted 1-Hydroxy-4-Sulfamoyl-2-Naphthoate Compounds Binding to Mcl1, Processes 7(4) (2019).

[59] Mai Suan Li, B.K. Mai, Steered Molecular Dynamics- A promising tools for drug design, Current Bioinformatics 7 (2012).

[60] Q. Liu, T. Moldoveanu, T. Sprules, E. Matta-Camacho, N. Mansur-Azzam, K. Gehring, Apoptotic regulation by MCL-1 through heterodimerization, J Biol Chem 285(25) (2010) 19615-24.

[61] M.L. Stewart, E. Fire, A.E. Keating, L.D. Walensky, The MCL-1 BH3 helix is an exclusive MCL-1 inhibitor and apoptosis sensitizer, Nature chemical biology 6(8) (2010) 595-601.